Thermal discrete dipole approximation for near-field radiative heat transfer in many-body systems with arbitrary nonreciprocal bodies

E. Moncada-Villa [1] and J. C. Cuevas [2]

[1]*Escuela de Física, Universidad Pedagógica y Tecnológica de Colombia, Avenida Central del Norte 39-115, Tunja, Colombia*
[2]*Departamento de Física Teórica de la Materia Condensada and Condensed Matter Physics Center (IFIMAC),*
Universidad Autónoma de Madrid, E-28049 Madrid, Spain

The theoretical study of many-body effects in the context of near-field radiative heat transfer (NFRHT) has already led to the prediction of a plethora of thermal radiation phenomena. Special attention has been paid to nonreciprocal systems in which the lack of the Lorentz reciprocity has been shown to give rise to unique physical effects. However, most of the theoretical work in this regard has been carried out with the help of approaches that consider either pointlike particles or highly symmetric bodies (such as spheres), which are not easy to realize and explore experimentally. In this work we develop a many-body approach based on the thermal discrete dipole approximation (TDDA) that is able to describe the NFRHT between nonreciprocal objects of arbitrary size and shape. We illustrate the potential and the relevance of this approach with the analysis of two related phenomena, namely the existence of persistent thermal currents and the photon thermal Hall effect, in a system with several magneto-optical bodies. Our many-body TDDA approach paves the way for closing the gap between experiment and theory that is hindering the progress of the topic of NFRHT in many-body systems.

I. INTRODUCTION

It is known that the Stefan-Boltzmann law sets an upper limit for the far field radiative thermal exchange between two bodies at different temperatures, which is valid for separations above the thermal wavelength ($\lambda_{th} \sim 9.6$ μm at room temperature). However, if the bodies are brought in closer proximity (below λ_{th}), the near-field radiative heat transfer (NFRHT) contribution arising from the evanescent field of electromagnetic waves at the material surfaces may lead to largely overcoming the blackbody limit. This near-field enhancement was first predicted by Polder and Van Hove back in 1971 [1] within the framework of the fluctuational electrodynamics (FE) [2], and in recent years it has been experimentally studied in a great variety of systems and using different types of materials [3–27]. These experiments, in turn, have been crucial to firmly establishing the basic NFRHT mechanisms in two-body systems; for recent reviews see Refs. [28,29].

In this context, part of the attention of the thermal radiation community has shifted to the investigation of many-body effects, a topic that is thus far largely dominated by the theory [30]. The NFRHT in many-body systems offers new exciting possibilities such as the development of functional devices, which are often the thermal radiation counterparts of electronic devices (diodes, transistors, etc.) [30,31]. On the other hand, many-body systems have also turned out to be ideal to unveil new physical phenomena that are absent in the standard two-body configuration. This is especially clear in the case of many-body systems involving nonreciprocal bodies, which are often based on magneto-optical (MO) objects whose near-field radiation properties can be largely tuned with

external magnetic fields [32–37]. Thus, for instance, in 2016 Ben-Abdallah predicted the possibility of having a near-field thermal analog of the Hall effect in an arrangement of four MO particles placed in a constant magnetic field [38]. Also in 2016, Zhou and Fan showed that a many-body system comprising MO nanoparticles can support a persistent directional heat current, without violating the second law of thermodynamics [39]. In fact, it has been shown that in certain systems these two striking phenomena are very much related and they should appear together [40].

The theoretical description of the NFRHT in nonreciprocal many-body systems has been restricted so far to either pointlike particles [38,41] or highly symmetric bodies [39,40,42]. Thus it would be desirable to extend the existing theoretical methods to describe the NFRHT in this type of system with bodies of arbitrary size and shape. This is exactly the goal of this work. To be precise, we present here an approach to deal with the NFRHT in nonreciprocal many-body systems made of objects of arbitrary size and shape which is based on an extension of the thermal discrete dipole approximation (TDDA) method that has been successful in describing the NFRHT of two-body systems [43,44], including those based on MO objects [34,45]. The TDDA approach, which is very much related to existing approaches to describe the radiative heat transfer in many-body systems of point dipoles [46,47], is based on a natural extension of the discrete dipole approximation (DDA) that is widely used for describing the scattering and absorption of light by small particles [48–51]. We shall illustrate here the power of our many-body TDDA method by analyzing both the photon Hall effect and the existence of a
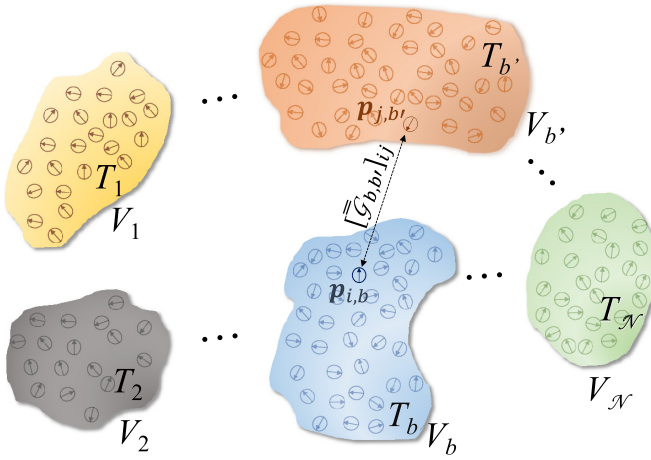
FIG. 1. Schematic representation of a generic many-body system consisting of $\mathcal{N}$ anisotropic bodies, each one at a temperature T_b and with a total volume V_b, described by a collection of N_b electrical point dipoles, $\mathbf{p}_{i,b}$, with a volume $V_{i,b}$ and dielectric permittivity tensor $\hat{\varepsilon}_{i,b}$.

persistent heat current in a system of MO particles beyond the standard point-dipole approximation. In particular, in the case of the photon Hall effect, our theory shows the need to amend the results of the original work of Ref. [38], as already pointed out in Ref. [35], and we show that the appearance of this effect in particles of finite size does not require extremely high magnetic fields.

The remainder of this paper is organized as follows. In Sec. II we present the many-body formalism based on the TDDA approach that enables us to describe the NFRHT between nonreciprocal bodies of arbitrary size and shape. Section III is devoted to the application of this formalism to the description of the photon thermal Hall effect and the appearance of a persistent heat current in a system comprised of four MO spherical particles. Finally, we summarize our main results in Sec. IV and discuss possible future research lines.

II. RADIATIVE HEAT EXCHANGE IN A SYSTEM WITH ARBITRARY ANISOTROPIC BODIES

The goal of this paper is to extend the TDDA approach to describe the near-field radiative heat transfer in many-body systems containing optically anisotropic bodies of arbitrary size and shape. We start by considering a system of $\mathcal{N}$ anisotropic bodies, as depicted in Fig. 1, each one having its own temperature T_b (the same throughout the body) and volume V_b. To describe this system we make use of the DDA [52], in which each body b is discretized in terms of a collection of N_b electrical point dipoles of volume $V_{i,b}$, dielectric permittivity tensor $\hat{\varepsilon}_{i,b}$, and polarizability

$$\hat{\alpha}_{i,b} = \left[\frac{1}{V_{i,b}} (\hat{L}_{i,b} + [\hat{\varepsilon}_{i,b} - \hat{1}]^{-1}) - i \frac{k_0^3}{6\pi} \hat{1} \right]^{-1}, \quad (1)$$

where $\hat{L}_j$ is the so-called depolarization tensor [53,54], which for cubic volume elements is diagonal and equal to $(1/3)\hat{1}$. The computation of the radiative heat transfer between the $\mathcal{N}$ bodies starts with the calculation of the statistical average of

the power dissipated in a particular body b due to the emission of the $\mathcal{N} - 1$ remaining bodies [45], that is

$$\mathcal{P}_b = \int_{V_b} \langle \bar{\mathbf{J}}_b(t) \cdot \bar{\mathbf{E}}_b(t) \rangle d\mathbf{r} = \left\langle \frac{d\bar{\mathbf{P}}_b(t)}{dt} \cdot \bar{\mathbf{E}}_b(t) \right\rangle, \quad (2)$$

where $\bar{\mathbf{P}}_b = (\mathbf{p}_1, \mathbf{p}_2, \ldots, \mathbf{p}_{N_b})^{\mathrm{T}}$ is a column supervector of dimension $3N_b \times 1$, whose components are the N_b electrical point dipolar moments in body b, the $3N_b \times 1$ supervector $\bar{\mathbf{E}}_b = (\mathbf{E}_1, \mathbf{E}_2, \ldots, \mathbf{E}_{N_b})^{\mathrm{T}}$ contains all the internal electric fields in each of the elementary volumes, and $\bar{\mathbf{J}}_b(t)$ contains all the local current densities related to the each electrical point dipole. For time harmonic fields, the absorbed power of Eq. (2) can be written as

$$\mathcal{P}_b = 2 \int_0^\infty \frac{d\omega}{2\pi} \omega \int_0^\infty \frac{d\omega'}{2\pi} \text{Im} \, \text{Tr} \{ \langle \bar{\mathbf{E}}_b^\dagger(\omega') \bar{\mathbf{P}}_b(\omega) \rangle e^{-i(\omega-\omega')t} \}, \quad (3)$$

where, for mathematical convenience, we use $\text{Tr} \{ \bar{\mathbf{E}}_b^\dagger(\omega') \bar{\mathbf{P}}_b(\omega) \}$ instead of $\bar{\mathbf{P}}_b(\omega) \cdot \bar{\mathbf{E}}_b^*(\omega')$. Each internal dipolar field contained in the vector $\bar{\mathbf{E}}_b$ appearing in Eq. (3) has contributions from all dipolar moments in the system. Within the DDA approach, the self-consistent volume integral equations relating the internal fields and the dipolar moments for all the $\mathcal{N}$ objects adopt the following matrix form [45,52]:

$$\bar{\bar{\mathbf{E}}} = \frac{k_0^2}{\varepsilon_0} \bar{\bar{\mathcal{G}}} \, \bar{\bar{\mathbf{P}}}, \quad (4)$$

where $\bar{\bar{\mathbf{E}}} = (\bar{\mathbf{E}}_1, \bar{\mathbf{E}}_2, \ldots, \bar{\mathbf{E}}_{\mathcal{N}})^{\mathrm{T}}$ and $\bar{\bar{\mathbf{P}}} = (\bar{\mathbf{P}}_1, \bar{\mathbf{P}}_2, \ldots, \bar{\mathbf{P}}_{\mathcal{N}})^{\mathrm{T}}$. Notice that $\bar{\bar{\mathbf{E}}}$ and $\bar{\bar{\mathbf{P}}}$ are $(\sum_{b=1}^{\mathcal{N}} 3N_b) \times 1$ supervectors containing, respectively, the internal electric fields and the dipolar moments of all the electric point dipoles in the $\mathcal{N}$-body system. In the matrix system of Eq. (4), $k_0 = \omega/c$ and ε_0 are, respectively, the vacuum wave vector and electric permittivity. Moreover, the quantity $\bar{\bar{\mathcal{G}}}$ denotes the dyadic Green's function matrix whose elements, connecting the ith dipolar moment inside the body b with the jth dipolar moment of body b' (see Fig. 1) and its elements, are given by

$$[\bar{\bar{\mathcal{G}}}_{b,b'}]_{ij} = \begin{cases} -\frac{\hat{L}_{i,b}}{V_{i,b}k_0^2} + \frac{ik_0}{6\pi}\hat{1}, & \text{if } i = j \text{ and } b = b', \\ [\hat{G}_{b,b'}]_{ij}, & \text{otherwise,} \end{cases} \quad (5)$$

where

$$[\hat{G}_{b,b'}]_{ij} = \frac{e^{ik_0R}}{4\pi R} \left[\left(1 + \frac{ik_0R - 1}{(k_0R)^2} \right) \hat{1} + \left(\frac{3 - 3ik_0R - (k_0R)^2}{(k_0R)^2} \right) \frac{\mathbf{R} \otimes \mathbf{R}}{R^2} \right], \quad (6)$$

and $\mathbf{R} = \mathbf{r}_{i,b} - \mathbf{r}_{j,b'}$. In problems like ours, where we are interested in the radiative heat exchange, the electrical dipoles have two basic contributions—one is a fluctuating one related to the thermal emission and the second one is an induced part related to the interactions between dipoles. Therefore, the total dipole moments can be written as [46]

$$\bar{\bar{\mathbf{P}}} = \bar{\bar{\mathbf{P}}}^{(\text{ind})} + \bar{\bar{\mathbf{P}}}^{(\text{fl})}. \quad (7)$$

Thus, in order to compute the thermal average of $\text{Tr} \{ \bar{\mathbf{E}}_b^\dagger(\omega') \bar{\mathbf{P}}_b(\omega) \}$ in Eq. (3), our task now is to express the quantities $\bar{\bar{\mathbf{E}}}_b$ and $\bar{\bar{\mathbf{P}}}_b$ in terms of the fluctuating parts of

the dipolar moments, whose properties are known (via the fluctuation-dissipation theorem). For this purpose, let us start by pointing out that the induced part of the local dipole moment is caused by all the local fields but its own, that is,

$$\bar{\bar{\mathbf{P}}}^{(\text{ind})} = \varepsilon_0 \bar{\bar{\alpha}} \bar{\bar{\mathbf{E}}}_{\text{exc}}, \tag{8}$$

where $\bar{\bar{\alpha}} = \text{diag}(\bar{\alpha}_1, \bar{\alpha}_2, \ldots, \bar{\alpha}_{\mathcal{N}})$ is a block-diagonal matrix with dimensions $(\sum_{b=1}^{\mathcal{N}} 3N_b) \times (\sum_{b=1}^{\mathcal{N}} 3N_b)$, whose elements are the $3N_b \times 3N_b$ block diagonal matrices $\bar{\alpha}_b = \text{diag}(\hat{\alpha}_{1,b}, \hat{\alpha}_{2,b}, \ldots, \hat{\alpha}_{N_b,b})$ and $\hat{\alpha}_{i,b}$ are the electrical polarizabilities given by Eq. (1). The exciting field, $\bar{\bar{\mathbf{E}}}_{\text{exc}}$, can be obtained after the subtraction of the self-interaction terms from the total internal field $\bar{\bar{\mathbf{E}}}$ as follows:

$$\bar{\bar{\mathbf{E}}}_{\text{exc}} = \frac{k_0^2}{\varepsilon_0} \Delta \bar{\bar{\mathcal{G}}} \, \bar{\bar{\mathbf{P}}}, \tag{9}$$

where $\Delta \bar{\bar{\mathcal{G}}} = \bar{\bar{\mathcal{G}}} - \text{diag}(\bar{\bar{\mathcal{G}}})$. Insertion of this exciting field into Eq. (8) leads to the following expression for the induced dipolar moment:

$$\bar{\bar{\mathbf{P}}}^{(\text{ind})} = k_0^2 \bar{\bar{\alpha}} \Delta \bar{\bar{\mathcal{G}}} \, \bar{\bar{\mathbf{P}}}, \tag{10}$$

from which, with the aid of Eq. (7), one obtains

$$\bar{\bar{\mathbf{P}}} = \bar{\bar{T}}^{-1} \bar{\bar{\mathbf{P}}}^{(\text{fl})}, \tag{11}$$

where $\bar{\bar{T}} = \hat{1} - k_0^2 \bar{\bar{\alpha}} \Delta \bar{\bar{\mathcal{G}}}$. From this, one arrives at the desired relation between the dipolar moments in the body b and the fluctuating part of all the dipoles of the $\mathcal{N}$-body system

$$\bar{\mathbf{P}}_b = \sum_{b'} [\bar{\bar{T}}^{-1}]_{bb'} \bar{\mathbf{P}}_{b'}^{(\text{fl})}. \tag{12}$$

At this point, we still have to calculate the internal fields in the body b, $\bar{\mathbf{E}}_b$, in terms of the fluctuating part of all the dipoles in the $\mathcal{N}$-body system. In what follows, we present two different, but equivalent ways in which this calculation can be done.

A. Method 1

As a first approach, we follow a line of reasoning similar to that used by Messina *et al.* in Ref. [46] for pointlike particles. In this case, we start by inserting the relation of Eq. (11) in Eq. (4) to obtain

$$\bar{\bar{\mathbf{E}}} = \frac{1}{\varepsilon_0} \bar{\bar{\mathcal{C}}} \, \bar{\mathbf{P}}^{(\text{fl})}, \tag{13}$$

from which

$$\bar{\mathbf{E}}_b^\dagger = \frac{1}{\varepsilon_0} \sum_{b'} \bar{\mathbf{p}}_{b'}^{(\text{fl})\dagger} [\bar{\bar{\mathcal{C}}}^\dagger]_{b'b}, \tag{14}$$

with $\bar{\bar{\mathcal{C}}} = k_0^2 \bar{\bar{\mathcal{G}}} \, \bar{\bar{T}}^{-1}$. The previous relation, together with Eq. (12), allows us to write the net power in Eq. (3) as

$$\mathcal{P}_b = \frac{2}{\varepsilon_0} \sum_{b',b''} \int_0^\infty \frac{d\omega}{2\pi} \omega \int_0^\infty \frac{d\omega'}{2\pi} \text{Im} \, \text{Tr}\{[\bar{\bar{\mathcal{C}}}^\dagger]_{b'b} [\bar{\bar{T}}^{-1}]_{bb''}$$
$$\times \langle \bar{\mathbf{p}}_{b''}^{(\text{fl})}(\omega') \bar{\mathbf{p}}_{b'}^{(\text{fl})\dagger}(\omega) \rangle e^{-i(\omega - \omega')t}\}. \tag{15}$$

The statistical average appearing in the preceding equation is given by the fluctuation dissipation theorem [55–57]

$$\langle \bar{\mathbf{p}}_{b''}^{(\text{fl})}(\omega') \bar{\mathbf{p}}_{b'}^{(\text{fl})\dagger}(\omega) \rangle = 4\pi \hbar \varepsilon_0 \delta_{b''b'} \delta(\omega - \omega') n_{\text{B}}(\omega, T_{b'}) \bar{\chi}_{b'}, \tag{16}$$

where $n_{\text{B}}(\omega, T_{b'}) = 1/(e^{\hbar\omega/k_{\text{B}}T_{b'}} - 1)$ is the Bose function, $\bar{\chi}_{b'} = \text{diag}(\hat{\chi}_{1,b'}, \hat{\chi}_{2,b'}, \ldots, \hat{\chi}_{N_{b'},b'})$, and

$$\hat{\chi}_{j,b} = \frac{1}{2i}(\hat{\alpha}_{j,b} - \hat{\alpha}_{j,b}^\dagger) - \frac{k_0^3}{6\pi} \hat{\alpha}_{j,b}^\dagger \hat{\alpha}_{j,b} \tag{17}$$

is the susceptibility of the jth dipole inside the body b. Introducing Eq. (16) into Eq. (15) we can simplify the expression for the net power received by the body b as follows:

$$\mathcal{P}_b = 4 \sum_{b'} \int_0^\infty \frac{d\omega}{2\pi} \hbar \omega n_{\text{B}}(\omega, T_{b'}) \text{Im} \, \text{Tr}\{[\bar{\bar{\mathcal{C}}}^\dagger]_{b'b} [\bar{\bar{T}}^{-1}]_{bb'} \bar{\chi}_{b'}\}. \tag{18}$$

In thermal equilibrium, when $T_b = T$ for all b, $\mathcal{P}_b$ must vanish, which implies that the following relation must hold:

$$\text{Im} \, \text{Tr}\{[\bar{\bar{\mathcal{C}}}^\dagger]_{bb} [\bar{\bar{T}}^{-1}]_{bb} \bar{\chi}_b\} = -\sum_{b' \neq b} \text{Im} \, \text{Tr}\{[\bar{\bar{\mathcal{C}}}^\dagger]_{b'b} [\bar{\bar{T}}^{-1}]_{bb'} \bar{\chi}_{b'}\}, \tag{19}$$

which allows us to write the net power in Eq. (18) as

$$\mathcal{P}_b = \sum_{b' \neq b} \mathcal{P}_{bb'}$$
$$= \sum_{b' \neq b} \int_0^\infty \frac{d\omega}{2\pi} [\Theta(\omega, T_{b'}) - \Theta(\omega, T_b)] \tau_{bb'}, \tag{20}$$

where $\Theta(\omega, T_b) = \hbar \omega n_{\text{B}}(\omega, T_b)$ and $\tau_{bb'}$ is the transmission probability between bodies b and b', which is given by

$$\tau_{bb'} = 4 \, \text{Im} \, \text{Tr}\{[\bar{\bar{\mathcal{C}}}^\dagger]_{b'b} [\bar{\bar{T}}^{-1}]_{bb'} \bar{\chi}_{b'}\}. \tag{21}$$

Notice that transmission probability of Eq. (21) is different from that reported in Ref. [38], which depends upon the imaginary part of the susceptibility instead of on the full susceptibility function. As we will illustrate in Sec. III, this difference leads to notable differences in the numerical results.

B. Method 2

Let us detail now an alternative way to compute the heat exchanges between the different bodies. In this case we use, instead of Eq. (4), the following relation between all the electric internal fields and the dipolar moments inside the body b:

$$\bar{\mathbf{E}}_b = \bar{\beta}_b \bar{\mathbf{P}}_b, \tag{22}$$

with

$$\bar{\beta}_b = \frac{1}{\varepsilon_0} \text{diag}\left(\frac{1}{V_{1,b}} [\hat{\varepsilon}_{1,b} - \hat{1}]^{-1}, \ldots, \frac{1}{V_{N_b,b}} [\hat{\varepsilon}_{N_b,b} - \hat{1}]^{-1}\right). \tag{23}$$

This relation, together with Eq. (12) for the fluctuating part of the dipolar moment, allows us to write the dissipated power in

body b, see Eq. (3), as

$$\mathcal{P}_b = 2 \sum_{b'b''} \int_0^\infty \frac{d\omega}{2\pi} \omega \int_0^\infty \frac{d\omega'}{2\pi} \text{Im Tr}\{[\bar{\bar{T}}^{-1}]_{b'b}^\dagger \bar{\beta}_b^\dagger [\bar{\bar{T}}^{-1}]_{bb''}$$

$$\times \langle \bar{\mathbf{P}}_{b''}^{(\text{fl})}(\omega') \bar{\mathbf{P}}_{b'}^{(\text{fl})\dagger}(\omega) \rangle e^{-i(\omega-\omega')t}\}. \quad (24)$$

Using again the fluctuation dissipation theorem, see Eq. (16), we can write the previous relation as

$$\mathcal{P}_b = 4\varepsilon_0 \sum_{b'} \int_0^\infty \frac{d\omega}{2\pi} \Theta(\omega, T_{b'}) \text{Im Tr}\{[\bar{\bar{T}}^{-1}]_{b'b}^\dagger \bar{\beta}_b^\dagger$$

$$\times [\bar{\bar{T}}^{-1}]_{bb'} \bar{\chi}_{b'}\},$$

$$= 4 \sum_{b'} \int_0^\infty \frac{d\omega}{2\pi} \Theta(\omega, T_{b'}) \text{Tr}\left\{[\bar{\bar{T}}^{-1}]_{b'b}^\dagger \frac{\varepsilon_0}{2i}(\bar{\beta}_b^\dagger - \bar{\beta}_b)\right.$$

$$\left. \times [\bar{\bar{T}}^{-1}]_{bb'} \bar{\chi}_{b'}\right\}. \quad (25)$$

Additionally, it is straightforward to show that $\frac{\varepsilon_0}{2i}(\bar{\beta}_b^\dagger - \bar{\beta}_b) = (\bar{\alpha}_b^\dagger)^{-1} \bar{\chi}_b \bar{\alpha}_b^{-1}$, and therefore the net power absorbed by the body b can be written as in Eq. (20), but with the following expression for the transmission probability:

$$\tau_{bb'} = 4 \text{Tr}\{\bar{\alpha}_b^{-1}[\bar{\bar{T}}^{-1}]_{bb'} \bar{\chi}_{b'} [\bar{\bar{T}}^{-1}]_{b'b}^\dagger (\bar{\alpha}_b^\dagger)^{-1} \bar{\chi}_b\}. \quad (26)$$

As will be shown in the next section, the numerical results obtained with this relation are identical to those obtained with Eq. (21). Furthermore, we would like to point out that, for a system consisting of only two arbitrary optically anisotropic bodies, the previous relation reduces to

$$\tau_{bb'} = 4k_0^4 \text{Tr}\{\bar{C}_{21} \bar{\chi}_1 \bar{C}_{21}^\dagger \bar{\chi}_2\}, \quad (27)$$

with

$$\bar{C}_{21} = \bar{D}_{22} \Delta \bar{\bar{\mathcal{G}}}_{21} [\hat{1} - k_0^2 \bar{\alpha}_1 \Delta \bar{\bar{\mathcal{G}}}_{11}]^{-1}, \quad (28)$$

$$\bar{D}_{22} = [\hat{1} - k_0^2 \Delta \bar{\bar{\mathcal{G}}}_{22} \bar{\alpha}_2$$

$$- k_0^4 \Delta \bar{\bar{\mathcal{G}}}_{21} \bar{\alpha}_1 [1 - k_0^2 \Delta \bar{\bar{\mathcal{G}}}_{11} \bar{\alpha}_1]^{-1} \Delta \bar{\bar{\mathcal{G}}}_{12} \bar{\alpha}_2]^{-1}, \quad (29)$$

$\bar{\bar{D}} = (\hat{1} - k_0^2 \Delta \bar{\bar{\mathcal{G}}} \bar{\bar{\alpha}})^{-1}$, and $\bar{\mathcal{G}}_{bb'}$ defined in Eq. (6). This expression agrees with the result of Eq. (57) reported in Ref. [45] for the two-body case. Let us stress that there is no doubt that Eqs. (26) and (21) must be identical and that one should be able to transform one into the other by simple algebraic manipulations. We have failed, though, to show this analytically, but we have numerically tested the equivalence of those two expressions in multiple situations, as we illustrate in Sec. III.

III. APPLICATION TO THE ANALYSIS OF THE PHOTON THERMAL HALL EFFECT AND THE PERSISTENT HEAT CURRENT

In this section we illustrate the use of the TDDA approach described in Sec. II with the analysis of two related many-body phenomena that occur with MO objects, namely the photon Hall effect and the possibility of having a persistent heat current. For this purpose, and following Ref. [38], we consider the system depicted in Fig. 2(a) that comprises four identical and spherical particles made of the n-doped semiconductor indium antimonide (InSb). These particles are
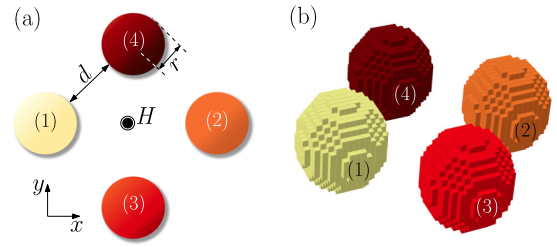
FIG. 2. (a) Schematic representation of the system under study, consisting of four magneto-optical spheres of radius r, placed in the vertices of a square in the xy plane, and under the action of a static magnetic field H along the positive z direction. (b) Discretization of each sphere as a collection of N_b of cubic point dipoles used to employ the approach of Sec. II.

eventually under the action of an external magnetic field along the positive z direction, which makes these particles nonreciprocal (see below). In the remainder of this paper, we shall assume these particles to be placed at the vertices of a square with a separation $d = 20$ nm and assume that they have a radius of $r = 100$ nm. As demonstrated in Ref. [38], if one creates a temperature difference $\Delta T = T_1 - T_2$ between particles 1 and 2, see Fig. 2, the presence of an external magnetic field will cause particles 3 and 4, whose temperatures are left free, to be different ($T_3 \neq T_4$), which is the near-field thermal analog of the electronic Hall effect. The magnitude of this Hall effect can be evaluated using the relative Hall temperature difference

$$R = \frac{T_3 - T_4}{T_1 - T_2}. \quad (30)$$

In the linear response regime, in which ΔT is infinitesimally small, it can be shown that R can be expressed as [38,58]

$$R = \frac{g_{13} - g_{31}}{g_{13} + g_{31} + 2g_{34}}, \quad (31)$$

where $g_{bb'}$ is the linear conductance between bodies b and b' at an equilibrium temperature T given by

$$g_{bb'} = \frac{\partial \mathcal{P}_{bb'}}{\partial T} = \int_0^\infty \frac{d\omega}{2\pi} \frac{\partial \Theta(\omega, T)}{\partial T} \tau_{bb'}(\omega). \quad (32)$$

In the previous expression, we identify

$$g_{bb'}(\omega) = \frac{1}{2\pi} \frac{\partial \Theta(\omega, T)}{\partial T} \tau_{bb'}(\omega) \quad (33)$$

as the thermal conductance per frequency interval or spectral thermal conductance. It is worth mentioning that the difference $g_{13} - g_{31}$ is proportional to the heat persistent current, which in turn is linked to the thermal Hall effect in nonreciprocal systems as well as in reciprocal ones with broken-mirror symmetry [40].

To compute the relative Hall thermal temperature difference we need to describe the optical properties of these MO particles in the presence of a magnetic field. Following Ref. [59], we assume that the InSb particles become nonreciprocal and their field-dependent dielectric tensor is given by

$$\hat{\epsilon} = \begin{pmatrix} \epsilon_1 & -i\epsilon_2 & 0 \\ i\epsilon_2 & \epsilon_1 & 0 \\ 0 & 0 & \epsilon_3 \end{pmatrix}, \quad (34)$$
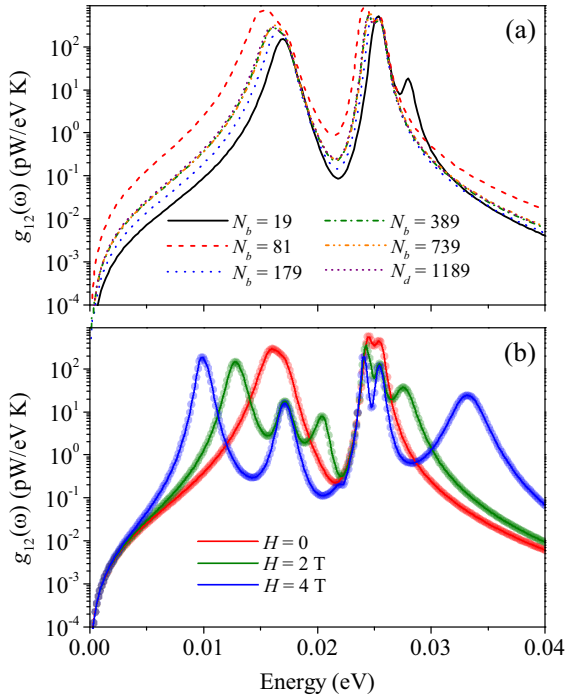
FIG. 3. (a) Zero-field spectral conductance as a function of the energy for spheres of a radius $r = 100$ nm and separated by a vacuum gap of $d = 20$ nm, for different values of the number of dipoles (see Fig. 2). (b) Spectral conductance for the same geometrical parameters in panel (a), with a fixed number of point dipoles ($N_b = 389$). Continuous lines correspond to transmission probability calculated with Eq. (21), whereas the circles correspond to the results obtained with Eq. (26). Room temperature (300 K) was assumed for all calculations in this work.

where

$$\epsilon_1(H) = \epsilon_\infty \left(1 + \frac{\omega_L^2 - \omega_T^2}{\omega_T^2 - \omega^2 - i\Gamma\omega} + \frac{\omega_p^2(\omega + i\gamma)}{\omega[\omega_c^2 - (\omega + i\gamma)^2]} \right),$$

$$\epsilon_2(H) = \frac{\epsilon_\infty \omega_p^2 \omega_c}{\omega[(\omega + i\gamma)^2 - \omega_c^2]},$$

$$\epsilon_3 = \epsilon_\infty \left(1 + \frac{\omega_L^2 - \omega_T^2}{\omega_T^2 - \omega^2 - i\Gamma\omega} - \frac{\omega_p^2}{\omega(\omega + i\gamma)} \right). \quad (35)$$

Here, ϵ_∞ is the high-frequency dielectric constant, ω_L (ω_T) is the longitudinal (transverse) optical phonon frequency, $\omega_p^2 = n e^2 / (m^* \epsilon_0 \epsilon_\infty)$ is the plasma frequency of free carriers of density n and effective mass m^*, Γ (γ) is the phonon (free-carrier) damping constant, and $\omega_c = eH/m^*$ is the cyclotron frequency, which depends on the intensity of the external magnetic field. For the moment, we assume the following room-temperature parameter values taken from Ref. [59]: $\epsilon_\infty = 15.7$, $\omega_L = 3.62 \times 10^{13}$ rad/s, $\omega_T = 3.39 \times 10^{13}$ rad/s, $\Gamma = 5.65 \times 10^{11}$ rad/s, $\gamma = 3.39 \times 10^{12}$ rad/s, $n = 1.07 \times 10^{17}$ cm^{-3}, $m^*/m = 0.022$, and $\omega_p = 3.14 \times 10^{13}$ rad/s.

We start the analysis of our results by exploring the convergence of our method. In Fig. 3(a), we show the spectral heat conductance $g_{12}(\omega)$ from body 1 to 2, see Fig. 2, calculated
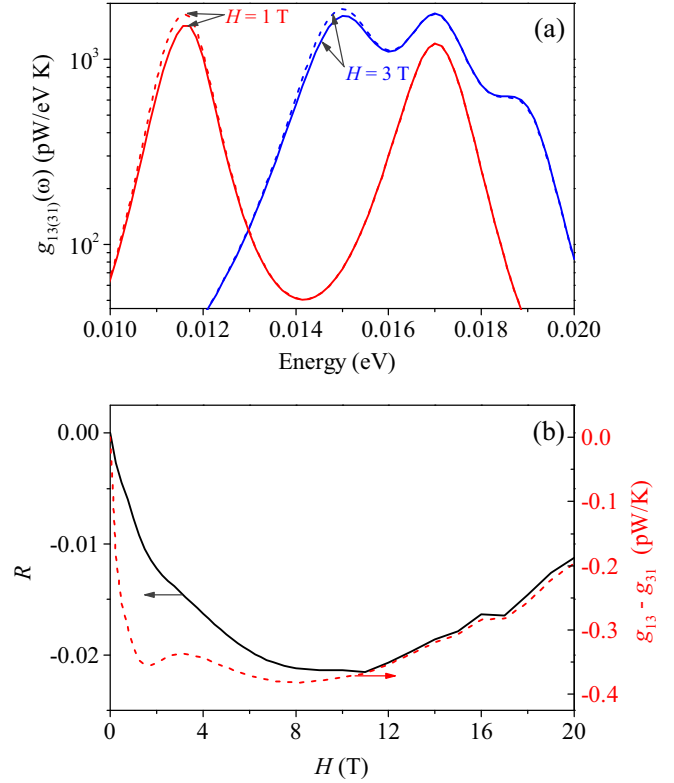
FIG. 4. (a) Spectral conductance $g_{13}(\omega)$ from the spheres 1 to 3 (solid lines), and from 3 to 1, $g_{31}(\omega)$ (dashed lines), as a function of the photon energy, for two different values of applied magnetic field. (b) Hall coefficient, Eq. (31), and persistent heat current $g_{13} - g_{31}$, Eq. (32), as a function of the applied magnetic field.

with the transmission probability of Eq. (21). In this case there is no external magnetic field and the different curves correspond to different numbers of point dipoles used to model each spherical particle. Notice the fast convergence of our method, which requires only 389 electrical point dipoles to reach convergence (within a relative error of 1%). The same convergence was obtained using Eq. (26) of method 2 (not shown here). It is worth mentioning that the method presented in this work is much more efficient than that of Ref. [45] for the two-body problem. To give a concrete example, in that work the authors reported that they required 4913 dipoles to converge the spectral conductance for two InSb cubes with sides of 1 μm and separated by a gap of 500 nm. For this same system, we only needed 343 dipoles to achieve a similar convergence with the methods presented here. Such a difference is due to the fact that in the current method [see Eqs. (21) and (26)] one does not do as many nested matrix operations as in Eqs. (27) and (28) (same equations reported in Ref. [45]), which avoids error propagation.

Once the convergence with the number of the point dipoles has been tested, we fix such a number to 389 and proceed to compare the results of the spectral heat transfer obtained with both transmission probabilities; see Eqs. (21) and (26). The results displayed in Fig. 3(b) show that, within the numerical accuracy, both methods give the same result for different values of the magnetic field. It is worth stressing that we have found this level of agreement for all the configurations
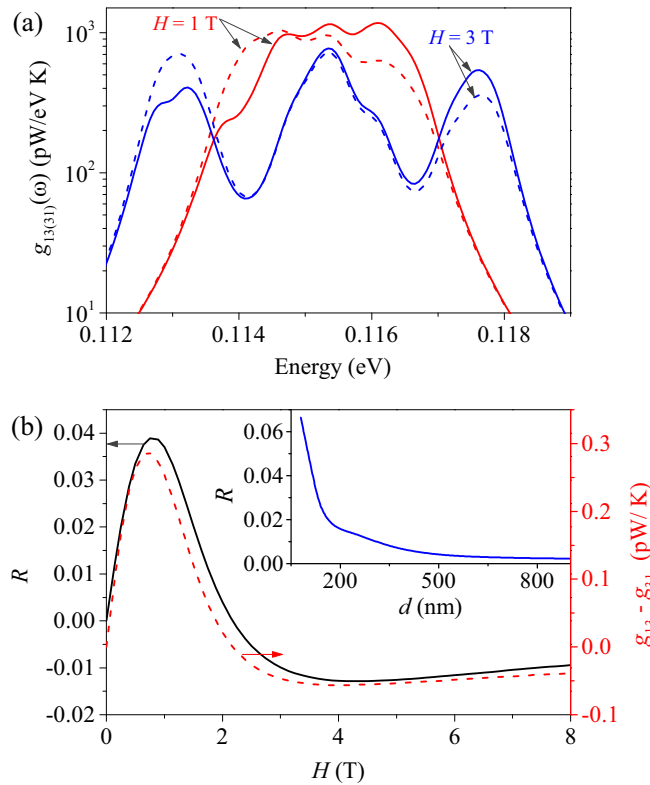
FIG. 5. Same as in Fig. 4, but for a vacuum gap of $d = 120$ nm, a plasma frequency $\omega_p = 1.86 \times 10^{14}$ rad/s, which corresponds to a higher doping level, $n = 1.36 \times 10^{19}$ cm^{-3}, and to an effective mass $m^* = 0.08m_e$ of the InSb. The inset in panel (b) shows the gap dependence of the Hall coefficient for an applied magnetic field of 1 T.

FIG. 6. Comparison between the arbitrary body approach Eq. (21) with $N_d = 389$ dipoles (continuous lines) and the result corresponding to a single point dipole (dashed lines), for different values of the static magnetic field. In both panels, spherical particles are assumed with a radius of 100 nm. Panels (a) and (b) correspond to gap values $d = 20$ nm and $d = 120$ nm, respectively.

investigated and, therefore, we conclude that these two methods are equivalent. With this in mind, all the results shown in what follows were obtained with transmission probability given by Eq. (21).

Now we can proceed to discuss the results of the photon thermal Hall effect that we obtain with our method. In Fig. 4(a) we present the spectral thermal conductance, in both directions, between bodies 1 and 3 at thermal equilibrium (see Fig. 2). These results show that the magnetic field induces a directional spectral conductance as a result of the effect of the induced optical anisotropy under the collective modes of the system. This effect, explained in Ref. [39] with the use of coupled mode theory, leads to both the existence of a heat persistent current at thermal equilibrium, characterized by the difference $g_{13} - g_{31}$, and the appearance of the photon thermal Hall effect, as is shown Fig. 4(b). As we pointed out in the preceding section, the difference between our analytical expression of Eq. (21) and that reported in Ref. [38] for pointlike particles leads to very different results for the Hall coefficient [see Fig. 4(b)]. This was already indicated in Ref. [35] making use of a theory for pointlike particles. In particular, we find that the occurrence of the photon thermal Hall signal requires more moderated intensities of the applied magnetic field than those reported in the original work, also in agreement with Ref. [35]. However, these field intensities are still relatively high due to the fact that the plasmonic

resonances of the particles, which are required for the directional collective modes in the system, are located in the region of the electromagnetic spectra where the InSb polaritonic band [ω_T, ω_L] is located. In order to enhance the sensitivity of the plasmonic resonances to the applied magnetic field, one can increase the carrier concentration in the InSb, and therefore the plasma frequency, as was done in Ref. [40]. Using a new plasma frequency of $\omega_p = 1.86 \times 10^{14}$ rad/s, one obtains a higher sensitivity of the spectral conductance between bodies 1 and 3 separated by a vacuum gap of $d = 120$ nm, as can be seen in Fig. 5(a), and, consequently, the persistent current and the photon thermal Hall effect occur for more moderate values of the magnetic field as evidenced in Fig. 5(b). Furthermore, in the inset of that panel, one can see that this effect is still appreciable for gap values up to 300 nm, for a magnetic field of 1 T. In addition, a comparison between Figs. 4(b) and 5(b) shows that by increasing the plasma frequency the direction of the persistent current can be reversed by the applied magnetic field. This is similar to what occurs for intrinsic nonreciprocal Weyl semimetals [58], for which the persistent current can flow either clockwise or counterclockwise depending on the strength of the nondiagonal elements of the dielectric tensor.

Finally, we use our method to test the validity of the pointlike approximation frequently used to analyze these many-body effects. For this purpose, in Fig. 6 we compare the results for the spectral thermal conductance between spheres 1 and 2 of Fig. 2 obtained with the approach developed in this work (solid lines) and those obtained assuming that the particles are pointlike (dashed lines) whose polarizability was calculated with the volume of the spheres. In this example all particles have the same radius of $r = 100$ nm and the vacuum gap is equal to $d = 20$ nm for panel (a) and $d = 120$ nm for panel (b). As expected, when $d < r$ as in panel (a), the pointlike approximation completely fails to reproduce the full numerical results and it only becomes an acceptable approximation when $d > r$ (and the size of the particle is much smaller than the thermal wavelength). However, in such a limit, effects such as the persistent current or the photon thermal Hall effect turn out to have very small amplitudes and they would be hard to measure in practice. This discussion illustrates the importance of using a method like the one presented in this work.

IV. CONCLUSIONS

Motivated by the recent interest in the NFRHT in many-body systems featuring nonreciprocal objects, in this work we have extended the TDDA approach to deal with any number of optically anisotropic bodies of arbitrary size and shape. We have illustrated this approach with the analysis of the photon thermal Hall effect and the appearance of a persistent current in a system comprising four MO spherical particles beyond the standard point-dipole approximation. In the case of the photon thermal Hall effect we have shown that the original analysis put forward in Ref. [38] has to be amended even in the limit of pointlike particles, as already explained in Ref. [35]. Moreover, our analysis shows that the Hall effect survives when finite particles are used and that it does not require magnetic fields as high as originally reported. On the other hand, as already discussed in Ref. [40], we have shown that the existence of the photon thermal Hall effect in our many-body system is naturally accompanied by the appearance of a persistent directional heat current that does not violate the second law of thermodynamics.

Our TDDA-based approach can be used for a great variety of problems and it can also be straightforwardly extended to deal with many different situations and phenomena. For instance, it is simple to adapt it to explore the nonadditivity of the thermal emission of many-body systems or to study the possibility of controlling such an emission with external magnetic fields (in the case of MO objects). On the other hand, since the TDDA is a volume-integral-equation method, our approach is also well suited to deal with more complex situations in which there are nontrivial temperature profiles across the objects or when those objects are made of a combination of materials (giving rise to space-dependent permittivities). For all those reasons, we think that the theoretical approach developed in this work is very valuable for the community of thermal radiation and photonics in general.

[1] D. Polder and M. Van Hove, Theory of radiative heat transfer between closely spaced bodies, Phys. Rev. B **4**, 3303 (1971).

[2] S. M. Rytov, Y. A. Kravtsov, and V. I. Tatarskii, *Principles of Statistical Radiophysics, Vol. 3: Elements of Random Fields* (Springer, Berlin, 1989).

[3] A. Kittel, W. Müller-Hirsch, J. Parisi, S.-A. Biehs, D. Reddig, and M. Holthaus, Near-Field Heat Transfer in a Scanning Thermal Microscope, Phys. Rev. Lett. **95**, 224301 (2005).

[4] A. Narayanaswamy, S. Shen, and G. Chen, Near-field radiative heat transfer between a sphere and a substrate, Phys. Rev. B **78**, 115303 (2008).

[5] L. Hu, A. Narayanaswamy, X. Y. Chen, and G. Chen, Near-field thermal radiation between two closely spaced glass plates exceeding Planck's blackbody radiation law, Appl. Phys. Lett. **92**, 133106 (2008).

[6] E. Rousseau, A. Siria, G. Jourdan, S. Volz, F. Comin, J. Chevrier, and J.-J, Greffet, Radiative heat transfer at the nanoscale, Nat. Photon. **3**, 514 (2009).

[7] S. Shen, A. Narayanaswamy, and G. Chen, Surface phonon polaritons mediated energy transfer between nanoscale gaps, Nano Lett. **9**, 2909 (2009).

[8] R. S. Ottens, V. Quetschke, S. Wise, A. A. Alemi, R. Lundock, G. Mueller, D. H. Reitze, D. B. Tanner, and B. F. Whiting, Near-Field Radiative Heat Transfer Between Macroscopic Planar Surfaces, Phys. Rev. Lett. **107**, 014301 (2011).

[9] S. Shen, A. Mavrokefalos, P. Sambegoro, and G. Chen, Nanoscale thermal radiation between two gold surfaces, Appl. Phys. Lett. **100**, 233114 (2012).

[10] T. Kralik, P. Hanzelka, M. Zobac, V. Musilova, T. Fort, and M. Horak, Strong Near-Field Enhancement of Radiative Heat Transfer Between Metallic Surfaces, Phys. Rev. Lett. **109**, 224302 (2012).

[11] P. J. van Zwol, L. Ranno, and J. Chevrier, Tuning Near Field Radiative Heat Flux Through Surface Excitations with a Metal Insulator Transition, Phys. Rev. Lett. **108**, 234301 (2012).

[12] P. J. van Zwol, S. Thiele, C. Berger, W. A. de Heer, and J. Chevrier, Nanoscale Radiative Heat Flow Due to Surface Plasmons in Graphene and Doped Silicon, Phys. Rev. Lett. **109**, 264301 (2012).

[13] B. Guha, C. Otey, C. B. Poitras, S. H. Fan, and M. Lipson, Near-field radiative cooling of nanostructures, Nano Lett. **12**, 4546 (2012).

[14] J. Shi, P. Li, B. Liu, and S. Shen, Tuning near field radiation by doped silicon, Appl. Phys. Lett. **102**, 183114 (2013).

[15] L. Worbes, D. Hellmann, and A. Kittel, Enhanced Near-Field Heat Flow of a Monolayer Dielectric Island, Phys. Rev. Lett. **110**, 134302 (2013).

[16] R. St-Gelais, B. Guha, L. X. Zhu, S. H. Fan, and M. Lipson, Demonstration of strong near-field radiative heat transfer between integrated nanostructures, Nano Lett. **14**, 6971 (2014).

[17] B. Song, Y. Ganjeh, S. Sadat, D. Thompson, A. Fiorino, V. Fernández-Hurtado, J. Feist, F. J. Garcia-Vidal, J. C. Cuevas, P. Reddy, and E. Meyhofer, Enhancement of near-field radiative heat transfer using polar dielectric thin films, Nat. Nanotechnol. **10**, 253 (2015).

[18] K. Kim, B. Song, V. Fernández-Hurtado, W. Lee, W. Jeong, L. Cui, D. Thompson, J. Feist, M. T. H. Reid, F. J. García-Vidal, J. C. Cuevas, E. Meyhofer, and P. Reddy, Radiative heat transfer in the extreme near field, Nature (London) **528**, 387 (2015).

[19] M. Lim, S. S. Lee, and B. J. Lee, Near-field thermal radiation between doped silicon plates at nanoscale gaps, Phys. Rev. B **91**, 195136 (2015).

[20] R. St-Gelais, L. Zhu, S. Fan, and M. Lipson, Near-field radiative heat transfer between parallel structures in the deep subwavelength regime, Nat. Nanotechnol. **11**, 515 (2016).

[21] B. Song, D. Thompson, A. Fiorino, Y. Ganjeh, P. Reddy, and E. Meyhofer, Radiative heat conductances between dielectric and metallic parallel plates with nanoscale gaps, Nat. Nanotechnol. **11**, 509 (2016).

[22] M. P. Bernardi, D. Milovich, and M. Francoeur, Radiative heat transfer exceeding the blackbody limit between macroscale planar surfaces separated by a nanosize vacuum gap, Nat. Commun. **7**, 12900 (2016).

[23] L. Cui, W. Jeong, V. Fernández-Hurtado, J. Feist, F. J. García-Vidal, J. C. Cuevas, E. Meyhofer, and P. Reddy, Study of radiative heat transfer in Ångström- and nanometre-sized gaps, Nat. Commun. **8**, 14479 (2017).

[24] K. Kloppstech, N. Könne, S.-A. Biehs, A. W. Rodriguez, L. Worbes, D. Hellmann, and A. Kittel, Giant heat transfer in the crossover regime between conduction and radiation, Nat. Commun. **8**, 14475 (2017).

[25] M. Ghashami, H. Geng, T. Kim, N. Iacopino, S.-K. Cho, and K. Park, Precision Measurement of Phonon-Polaritonic Near-Field Energy Transfer Between Macroscale Planar Structures Under Large Thermal Gradients, Phys. Rev. Lett. **120**, 175901 (2018).

[26] A. Fiorino, D. Thompson, L. Zhu, B. Song, P. Reddy, and E. Meyhofer, Giant enhancement in radiative heat transfer in sub-30 nm gaps of plane parallel surfaces, Nano Lett. **18**, 3711 (2018).

[27] J. DeSutter, L. Tang, and M. Francoeur, A near-field radiative heat transfer device, Nat. Nanotechnol. **14**, 751 (2019).

[28] B. Song, A. Fiorino, E. Meyhofer, and P. Reddy, Near-field radiative thermal transport: From theory to experiment, AIP Adv. **5**, 053503 (2015).

[29] J. C. Cuevas and F. J. García-Vidal, Radiative heat transfer, ACS Photon. **5**, 3896 (2018).

[30] S.-A. Biehs, R. Messina, P. S. Venkataram, A. W. Rodriguez, J. C. Cuevas, and P. Ben-Abdallah, Near-field radiative heat transfer in many-body systems, Rev. Mod. Phys. **93**, 025009 (2021).

[31] P. Ben-Abdallah and S. A. Biehs, Thermotronics: Towards nanocircuits to manage radiative heat flux, Z. Naturforsch. A **72**, 151 (2017).

[32] E. Moncada-Villa, V. Fernández-Hurtado, F. J. García-Vidal, A. García-Martín, and J. C. Cuevas, Magnetic field control of near-field radiative heat transfer and the realization of highly tunable hyperbolic thermal emitters, Phys. Rev. B **92**, 125418 (2015).

[33] I. Latella and P. Ben-Abdallah, Giant Thermal Magnetoresistance in Plasmonic Structures, Phys. Rev. Lett. **118**, 173902 (2017).

[34] R. M. Abraham Ekeroth, P. Ben-Abdallah, J. C. Cuevas, and García-Martín, Anisotropic thermal magnetoresistance for an active control of radiative heat transfer, ACS Photon. **5**, 705 (2018).

[35] A. Ott, R. Messina, P. Ben-Abdallah, and S.-A. Biehs, Magnetothermoplasmonics: from theory to applications, J. Photon. Energy **9**, 032711 (2019).

[36] E. Moncada-Villa and J. C. Cuevas, Magnetic field effects in the near-field radiative heat transfer between planar structures, Phys. Rev. B **101**, 085411 (2020).

[37] E. Moncada-Villa and J. C. Cuevas, Near-field radiative heat transfer between one-dimensional magnetophotonic crystals, Phys. Rev. B **103**, 075432 (2021).

[38] P. Ben-Abdallah, Photon Thermal Hall Effect, Phys. Rev. Lett. **116**, 084301 (2016).

[39] L. Zhu and S. Fan, Persistent Directional Current at Equilibrium in Nonreciprocal Many-Body Near Field Electromagnetic Heat Transfer, Phys. Rev. Lett. **117**, 134303 (2016).

[40] C. Guo, Y. Guo, and S. Fan, Relation between photon thermal Hall effect and persistent heat current in nonreciprocal radiative heat transfer, Phys. Rev. B **100**, 205416 (2019).

[41] A. Ott and S.-A. Biehs, Thermal rectification and spin-spin coupling of nonreciprocal localized and surface modes, Phys. Rev. B **101**, 155428 (2020).

[42] L. Zhu, Y. Guo, and S. Fan, Theory of many-body radiative heat transfer without the constraint of reciprocity, Phys. Rev. B **97**, 094302 (2018).

[43] S. Edalatpour and M. Francoeur, The Thermal Discrete Dipole Approximation (T-DDA) for near-field radiative heat transfer simulations in three-dimensional arbitrary geometries, J. Quant. Spectrosc. Radiat. Transfer **133**, 364 (2014).

[44] S. Edalatpour, M. Cuma, T. Trueax, R. Backman, and M. Francoeur, Convergence analysis of the thermal discrete dipole approximation, Phys. Rev. E **91**, 063307 (2015).

[45] R. M. Abraham Ekeroth, A. García-Martín, and J. C. Cuevas, Thermal discrete dipole approximation for the description of thermal emission and radiative heat transfer of magneto-optical systems, Phys. Rev. B **95**, 235428 (2017).

[46] R. Messina, M. Tschikin, S.-A. Biehs, and P. Ben-Abdallah, Fluctuation-electrodynamic theory and dynamics of heat transfer in systems of multiple dipoles, Phys. Rev. B **88**, 104307 (2013).

[47] E. Tervo, M. Francoeur, B. Cola, and Z. Zhang, Thermal radiation in systems of many dipoles, Phys. Rev. B **100**, 205422 (2019).

[48] E. M. Purcell and C. R. Pennypacker, Scattering and absorption of light by nonspherical dielectric grains, Astrophys. J. **186**, 705 (1973).

[49] B. T. Draine, The discrete-dipole approximation and its application to interstellar graphite grains, Astrophys. J. **333**, 848 (1988).

[50] B. T. Draine and P. J. Flatau, Discrete-dipole approximation for scattering calculations, J. Opt. Soc. Am. A **11**, 1491 (1994).

[51] M. A. Yurkin and A. G. Hoekstra, The discrete dipole approximation: An overview and recent developments, J. Quant. Spectrosc. Radiat. Transfer **106**, 558 (2007).

[52] L. Novotny and B. Hecht, *Principles of Nano-Optics* (Cambridge University Press, Cambridge, UK, 2012).

[53] A. Lakhtakia, General theory of the Purcell-Pennypacker scattering approach and its extension to bianisotropic scatterers, Astrophys. J. **394**, 494 (1992).

[54] A. D. Yaghjian, Electric dyadic Green's functions in the source region, Proc. IEEE **68**, 248 (1980).

[55] L. Landau, E. Lifshitz, and L. Pitaevskii, *Course of Theoretical Physics* (Pergamon, New York, 1980), Vol. 9, Part 2.

[56] Yu. A. Il'inskii and L. V. Keldysh, *Electromagnetic Response of Material Media* (Plenum Press, New York, 1994).

[57] K. Joulain, J.-P. Mulet, F. Marquier, R. Carminati, and J.-J. Greffet, Surface electromagnetic waves thermally excited: Radiative heat transfer, coherence properties and Casimir forces revisited in the near field, Surf. Sci. Rep. **57**, 59 (2005).

[58] A. Ott, S.-A. Biehs, and P. Ben-Abdallah, Anomalous photon thermal Hall effect, Phys. Rev. B **101**, 241411(R) (2020).

[59] E. D. Palik, R. Kaplan, R. W. Gammon, H. Kaplan, R. F. Wallis, and J. J. Quinn, Coupled surface magnetoplasmon-optic-phonon polariton modes on InSb, Phys. Rev. B **13**, 2497 (1976).